Hindawi
Complexity
Volume 2021, Article ID 5927070, 12 pages
https://doi.org/10.1155/2021/5927070

Research Article

Soret and Radiation Effects on Mixture of Ethylene Glycol-Water (50%-50%) Based Maxwell Nanofluid Flow in an Upright Channel

Kashif Sadiq,[1] Fahd Jarad,[2,3] Imran Siddique,[1] and Bagh Ali[4]

[1]*Department of Mathematics, University of Management and Technology, Lahore-54770, Pakistan*
[2]*Department of Mathematics, Cankaya University, Etimesgut, Ankara, Turkey*
[3]*Department of Medical Research, China Medical University Hospital, China Medical University, Taichung, Taiwan*
[4]*School of Mathematics and Statistics, Northwestern Polytechnical University, Xian 710129, China*

Correspondence should be addressed to Fahd Jarad; fahd@cankaya.edu.tr

Received 12 April 2021; Revised 4 May 2021; Accepted 18 May 2021; Published 27 May 2021

Academic Editor: Ali Akgül

In this article, ethylene glycol (EG) + waterbased Maxwell nanofluid with radiation and Soret effects within two parallel plates has been investigated. The problem is formulated in the form of partial differential equations. The dimensionless governing equations for concentration, energy, and momentum are generalized by the fractional molecular diffusion, thermal flux, and shear stress defined by the Caputo–Fabrizio time fractional derivatives. The solutions of the problems are obtained via Laplace inversion numerical algorithm, namely, Stehfest's. Nanoparticles of silver (Ag) are suspended in a mixture of EG + water to have a nanofluid. It is observed that the thermal conductivity of fluid is enhanced by increasing the values of time and volume fraction. The temperature and velocity of water-silver nanofluid are higher than those of ethylene glycol (EG) + water (H_2O)-silver (Ag) nanofluid. The results are discussed at 2% of volume fraction. The results justified the thermo-physical characteristics of base fluids and nanoparticles shown in the tables. The effects of major physical parameters are illustrated graphically and discussed in detail.

1. Introduction

Fluids like coolants (ethylene glycol and water), lubricants (oils), paraffin, biofluids, and polymer solutions are common conductive fluids. Nanofluids have better thermo-physical features such as viscosity, rate of heat transfer, thermal diffusion, and thermal conductivity compared with conventional fluids. Due to enhanced qualities, nanofluids have many applications in biomedical, engineering, and industries, for example, nanocryosurgery, magnetic drug, electronics cooling, vehicle cooling, smart fluids, industrial cooling, and heat transfer [1]. Heat exchangers, electric conductors, solar collectors, and piping are the most recent applications of heat transfer. These applications are used to reduce and enhance the heat of systems and depend on convection. Though, it is obvious that suitable fluids are essential for heat transfer.

Many researchers are investigating the Soret effect on natural convection mass and heat transport due to its applications in scientific systems and engineering. The gradients of temperature cause mass diffusion which is called the Soret effect. Isotopes separation, geosciences, hydrology, petrology, and chemical processing are applications of Soret effects [2–7]. RamReddy et al. [8] studied mass and heat transport in mixed convection nanofluid flow on a plate influenced by the Soret effect. Raju et al. [9] analyzed the nanofluid flow on a moving vertical plate influenced by magnetic field, thermal radiation, and Soret effect.

Ganesh et al. [10] investigated the flow of ethylene glycol ($C_2H_6O_2$) + water (H_2O) (50 : 50) comprising the nanoparticles of boehmite alumina with Sakiadis and Blasius slip. Arani et al. [11] applied the simple algorithm to analyze the flow of a mixture of $C_2H_6O_2$–H_2O (50 : 50) and different shapes of nanoparticles of boehmite alumina in a channel. They found that the nanoparticles of spherical shape affect the thermal conductivity significantly. Monfared et al. [12] studied the effects of shapes of nanoparticles of boehmite alumina on entropy generation and thermal conductivity on

the flow of a nanofluid in a heat exchanger double pipe. They concluded that the entropy generation has a maximum frictional rate for the nanoparticles of platelet shape. Nisar et al. [13] numerically investigated EG-water (50 : 50) based mixed convection hybrid nanofluid flow within two disks with thermal radiation.

In diverse problems of physical sciences and engineering integer, order or classical derivative cannot represent the complex dynamics conditions entirely. In these cases, the fractional-order derivatives are more suitable approaches, in viscous flows, biology, biomedical sciences, signal and image handling, chemical reaction, treatment, and cancer diagnosis. Fractional-order derivatives can demonstrate the memory results of flow and describe the traditional properties. It is significant to discuss that fractional derivatives have numerous applications in the field of modern technology and science which consists of viscoelasticity, relaxation process, diffusion, and electrochemistry [14]. Markis et al. [15] investigated the fractional model of Maxwell's fluid flow. They concluded that by changing the value of the fractional parameter, the results can be adjusted close to the experimental results. Zafer and Fetecau [16] used Caputo–Fabrizio fractional derivative to examine the Newtonian fluid flow on a vertical plate. Siddique and Bukhari [17] analyzed the effect of generalized fractional Fourier's and Fick's laws on convective flows of non-Newtonian fluid subject to Newtonian heating. Alkahtani and Atangana [18] applied diverse fractional methods to study heat transfer and memory effect. They developed new numerical techniques for the solution of fractional equations. Siddique et al. [19] studied the heat transfer analysis in convective flows of fractional second grade fluids with Caputo–Fabrizio and Atangana–Baleanu derivative subject to Newtonion heating. Abro et al. [20] calculated exact analytical results for Oldroyd-B fluid flow in a pipe. Siddique et al. [21] studied the unsteady flow of Walter's-B fluid subject to a consistent inclined magnetic field at an angle of inclination over the boundary of transverse xy-plane with fractional thermal transport. In this paper, they found the semianalytical solutions of the dimensionless temperature and velocity fields by using the Laplace inversion numerical algorithms such as Stehfest's and Tzou's. Vieru et al. [22] investigated the exact results of the flow of viscous fluid for the fractional model on a vertical plate with Newtonian heating and mass diffusion.

Motivated by the above study, focus of this work is to examine the flow of mass and heat in an unsteady Maxwell nanofluid flow inside two vertical parallel plates with combined effect of Soret and thermal radiation. The numerical inverse Laplace transform is used to compute the solutions of equations. The graphical illustration of the significant constraints on concentration, heat, and flow profiles is presented and discussed in detail. The fractional model of nanofluid is developed to generalize the standard constitutive equations by using equation of shear stress, Fourier's law, and molecular diffusion. It is obvious that most investigations considered water as base fluid. The inspiration of this examination is consequently to study the heat presentation of nanofluid using EG-water (50 : 50) as base fluid and nanoparticles of Ag. EG is a natural fluid of low instability and viscosity, which is totally mixable with water; hence, it very well may be utilized as a base fluid all alone or blended in with water to frame EG-water base fluid. The impacts of Soret effect on the concentration of fluid are additionally explored. The graphical description of the relevant parameters on the flow of fluid, mass, and heat exchange attributes is shown and completely examined.

2. Mathematical Model

An incompressible, unsteady, viscous 2D flow of Maxwell nanofluid within two infinite parallel plates having distance d between them in the presence of Soret and thermal radiation effects is considered. The nanofluid is prepared by adding nanoparticles of silver into the mixture of EG-water (50 : 50) at a fixed volume fraction ϕ. The Maxwell nanofluid is viewed as optically thick. Thus, the Rosseland estimations can be used for radiation impacts.

X-axis is taken along the plates and y-axis is taken normal to the plates as demonstrated in Figure 1. At first, both nanofluid and plates are in equilibrium at fixed temperature T_0 and concentration C_0.The right plate slides at $\tilde{t} \geq 0$ in the plane along x-axis with the velocity U_0. Simultaneously, concentration and temperature levels rise to C_1 and T_1. The radiative heat flux q_r is outlined in the temperature equation.

Thermo-physical features of EG-H_2O, H_2O, and silver are given in Table 1, which are assumed to be constant. It is also considered that the fluid and nanoparticles are in thermal stability, and slippage among them is neglected. The viscous diffusion in the heat equation is ignored because of its little size in natural convection flows in spite of the fact that it can lessen the heat presentation of nanofluids which changes with the rate of flow. Then again, the dissipating of nanoparticles in a fluid is joined by a development of the viscosity which diminishes its flow. Subsequently, the scattering of nanoparticles in a base fluid cannot be subjective. It must be investigated or even improved.

Since the boundaries of channel are infinitely long in the x- and z-axis, we can expect that all actual parameters describing heat transfer and the flow of fluid are elements of $\tilde{t}$ and $\tilde{y}$ only.

The equation of continuity is uniformly justified for the velocity field $\mathbf{v} = (\tilde{u}(\tilde{y}, \tilde{t}), 0, 0)$, and the typical Boussinesq's approximation is utilized. The expressions of the unsteady flow when pressure gradient is neglected are as follows [23]:

The linear momentum equation is as follows:

$$\rho_{nf} \frac{\partial \tilde{u}}{\partial \tilde{t}} = \frac{\partial \tilde{\tau}}{\partial \tilde{y}} + g(\rho\beta_T)_{nf}\left[\tilde{T} - T_0\right] + g(\rho\beta_C)_{nf}\left[\tilde{C} - C_0\right]. \tag{1}$$

The shear stress is as follows:

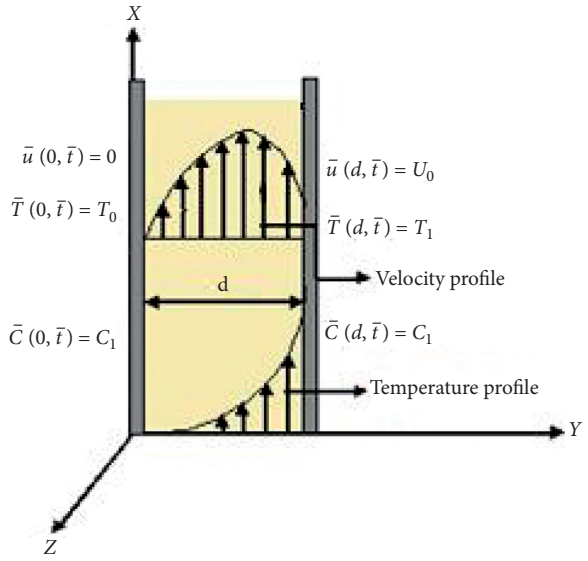

Figure 1: Flow geometry.

Table 1: Thermo-physical features of nanoparticles and EG [13].

Material	EG-H_2O (50 : 50)	H_2O	Silver (Ag)
ρ	1056	997.1	10500
c_p	3288	4179	235
k	0.425	0.613	429
$\beta \times 10^{-5}$	0.00341	21	1.89
Pr	29.86	6.2	—

$$\left(1 + \tilde{\lambda}\frac{\partial}{\partial \tilde{t}}\right)\tilde{\tau} = \mu_{nf}\frac{\partial \tilde{u}}{\partial \tilde{y}}. \tag{2}$$

The energy equation is as follows:

$$\left(\rho c_p\right)_{nf}\frac{\partial \tilde{T}}{\partial \tilde{t}} = -\frac{\partial \tilde{q}}{\partial \tilde{y}} - \frac{\partial q_r}{\partial \tilde{y}}. \tag{3}$$

The thermal flux is as follows:

$$\tilde{q} = -k_{nf}\frac{\partial \tilde{T}}{\partial \tilde{y}}. \tag{4}$$

The diffusion equation is as follows:

$$\frac{\partial \tilde{C}}{\partial \tilde{t}} = -\frac{\partial \tilde{j}}{\partial \tilde{y}} + \frac{D_{nf}k_T}{T_m}\frac{\partial^2 T}{\partial y^2}. \tag{5}$$

The molecular diffusion is as follows:

$$\tilde{j} = -D_{nf}\frac{\partial \tilde{C}}{\partial \tilde{y}}, \tag{6}$$

with corresponding conditions such as

$$\begin{aligned} &\tilde{u}(0,\tilde{t}) = 0, \\ &\tilde{u}(y,0) = 0, \\ &\tilde{u}(d,\tilde{t}) = U_0, \end{aligned} \tag{7}$$

$$\begin{aligned} &\tilde{T}(0,\tilde{t}) = T_0, \\ &\tilde{T}(y,0) = T_0, \\ &\tilde{T}(d,\tilde{t}) = T_1, \end{aligned} \tag{8}$$

$$\begin{aligned} &\tilde{C}(y,0) = C_0, \\ &\tilde{C}(0,\tilde{t}) = C_0, \\ &\tilde{C}(d,\tilde{t}) = C_1. \end{aligned} \tag{9}$$

The thermal-physical properties of nanofluid are defined by [24]

$$\begin{aligned}
\frac{\mu_{nf}}{\mu_f} &= \frac{1}{(1-\phi)^{2.5}},\\
\frac{\rho_{nf}}{\rho_f} &= (1-\phi)+\phi\frac{\rho_s}{\rho_f},\\
\frac{\left(\rho c_p\right)_{nf}}{\left(\rho c_p\right)_f} &= (1-\phi)+\phi\frac{\left(\rho c_p\right)_s}{\left(\rho c_p\right)_f},\\
\frac{D_{nf}}{D_f} &= \frac{1}{(1-\phi)},\\
\frac{(\rho\beta_T)_{nf}}{(\rho\beta_T)_f} &= (1-\phi)+\phi\frac{(\rho\beta_T)_s}{(\rho\beta_T)_f},\\
\frac{(\rho\beta_C)_{nf}}{(\rho\beta_C)_f} &= (1-\phi)+\phi\frac{(\rho\beta_C)_s}{(\rho\beta_C)_f},\\
\frac{k_{nf}}{k_f} &= \left[\frac{k_s+2k_f-2\phi\left(k_f-k_s\right)}{k_s+2k_f+\phi\left(k_f-k_s\right)}\right].
\end{aligned} \tag{10}$$

Introducing the dimensionless parameters, variables, and functions,

$$\begin{aligned}
u &= \frac{u}{U_0},\\
t &= \frac{\nu_f\tilde{t}}{d^2},\\
y &= \frac{y}{d},\\
\theta &= \frac{T-T_0}{T_1-T_0},\\
C &= \frac{C-C_0}{C_1-C_0},\\
\lambda &= \frac{\lambda\nu_f}{d^2},\\
q &= \frac{q}{q_0},\\
q_0 &= \frac{k_{nf}(T_1-T_0)}{d},\\
\tau &= \frac{\tilde{\tau}}{\tau_0},\\
\tau_0 &= \mu_{nf}\frac{U_0}{d},\\
j &= \frac{y}{j_0},\\
j_0 &= \frac{D_{nf}(C_1-C_0)}{d},
\end{aligned}$$

$$\begin{aligned}
a_1 &= \frac{\mu_{nf}}{\rho_{nf}\nu_f},\\
a_2 &= Gr\frac{(\beta_T)_{nf}}{(\beta_T)_f},\\
a_3 &= Gm\frac{(\beta_C)_{nf}}{(\beta_C)_f},\\
a_4 &= \frac{1}{\mathrm{Pr}}\frac{k_{nf}\left(\rho c_p\right)_f}{k_f\left(\rho c_p\right)_{nf}},\\
a_5 &= \frac{Nr}{\mathrm{Pr}}\frac{\left(\rho c_p\right)_f}{\left(\rho c_p\right)_{nf}},\\
a_6 &= \frac{1}{Sc}\frac{D_{nf}}{D_f},\\
a_7 &= Sr\frac{D_{nf}}{D_f},\\
Gr &= \frac{g(\beta_T)_f(T_1-T_0)d^2}{U_0\nu_f},\\
Sc &= \frac{\nu_f}{D_f},\\
Sr &= \frac{D_f k_T(T_1-T_0)}{T_m(C_1-C_0)\nu_f},\\
Gm &= \frac{g(\beta_C)_f(C_2-C_1)d^2}{U_0\nu_f},\\
Nr &= \frac{16\sigma' T_1^3}{3k'k_f},\\
\mathrm{Pr} &= \frac{\left(\rho c_p\right)_f\nu_f}{k_f},
\end{aligned} \tag{11}$$

where U_0, τ_0, q_0, and j_0 are characteristic scales.

By switching equation (11) into equations (1)–(9), we get

$$\frac{\partial u}{\partial t} = a_1\frac{\partial\tau}{\partial y}+a_2\theta+a_3C, \tag{12}$$

$$\left(1+\lambda\frac{\partial}{\partial t}\right)\tau = \frac{\partial u}{\partial y}, \tag{13}$$

$$\frac{\partial\theta}{\partial t} = -a_4\frac{\partial q}{\partial y}+a_5\frac{\partial^2\theta}{\partial y^2}, \tag{14}$$

$$q(y,t) = -\frac{\partial\theta}{\partial y}, \tag{15}$$

$$\frac{\partial C(y,t)}{\partial t} = -a_6\frac{\partial j(y,t)}{\partial y}+a_7\frac{\partial^2\theta}{\partial y^2}, \tag{16}$$

$$j(y,t) = -\frac{\partial C(y,t)}{\partial y}, \tag{17}$$

with corresponding conditions such as

$$\begin{aligned} u(y,0) &= 0, \\ u(0,t) &= 0, \\ u(1,t) &= 1, \end{aligned} \tag{18}$$

$$\begin{aligned} \theta(y,0) &= 0, \\ \theta(0,t) &= 0, \\ \theta(1,t) &= 1, \end{aligned} \tag{19}$$

$$\begin{aligned} C(y,0) &= 0, \\ C(0,t) &= 0, \\ C(1,t) &= 1. \end{aligned} \tag{20}$$

To discuss the time fractional derivative models, the researchers consider the developed generalization of the standard constitutive equations (13), (15), and (17) by using the equation of shear stress as follows:

$$\left(1 + \lambda \frac{\partial}{\partial t}\right)\tau(y,t) = -{}^{CF}D_t^{\alpha}\frac{\partial u(y,t)}{\partial y}, \quad 0 \le \alpha < 1. \tag{21}$$

Fourier's law is as follows:

$$q(y,t) = -{}^{CF}D_t^{\beta}\frac{\partial \theta(y,t)}{\partial y}, \quad 0 \le \beta < 1, \tag{22}$$

and Fick's law is as follows:

$$j(y,t) = -{}^{CF}D_t^{\gamma}\frac{\partial C(y,t)}{\partial y}, \quad 0 \le \gamma < 1. \tag{23}$$

In the above equations, ${}^{CF}D_t^{\zeta}(\cdot)$ represents the Caputo–Fabrizio time fractional derivative described by [25]

$${}^{CF}D_t^{\xi}\Psi(\eta,t) = \frac{1}{1-\xi}\int_0^t \exp\left(\frac{-\xi(t-\Omega)}{1-\xi}\right)\frac{\partial \Psi(\eta,\Omega)}{\partial \Omega}\,d\Omega, \quad 0 \le \xi < 1. \tag{24}$$

The Laplace transform of equation (24) is as follows:

$$L\left\{{}^{CF}D_t^{\xi}\Psi(\eta,t)\right\} = \frac{sL\{\Psi(\eta,t)\} - \Psi(\eta,0)}{(1-\xi)s + \xi}. \tag{25}$$

Remark. If $\Psi(\eta,0) = 0$ and $\xi \longrightarrow 0$, equation (25) becomes $L\left\{{}^{CF}D_t^{\xi}\Psi(\eta,t)\right\} = L\{\Psi(\eta,t)\}$. Then, generalized shear stress, thermal flux, and molecular diffusion equations (21)–(23) reduce to the classical equations (13), (15), and (17).

Eliminating $\tau$from (12) and (21), we get

$$\left(1 + \lambda \frac{\partial}{\partial t}\right)\frac{\partial u}{\partial t} = a_1\,{}^{CF}D_t^{\alpha}\frac{\partial^2 u}{\partial y^2} + a_2\left(1 + \lambda \frac{\partial}{\partial t}\right)\theta + a_3\left(1 + \lambda \frac{\partial}{\partial t}\right)C. \tag{26}$$

Eliminating $q$from (14) and (22), we get

$$\frac{\partial \theta}{\partial t} = a_4\,{}^{CF}D_t^{\beta}\frac{\partial^2 \theta}{\partial y^2} + a_5\frac{\partial^2 \theta}{\partial y^2}. \tag{27}$$

Now, eliminating j from (16) and (23), we have

$$\frac{\partial C}{\partial t} = a_6\,{}^{CF}D_t^{\gamma}\frac{\partial^2 C}{\partial y^2} + a_7\frac{\partial^2 \theta}{\partial y^2}. \tag{28}$$

3. Solution of the Problems

Applying the Laplace transform to equations (26)–(28) and using conditions (18)–(20), we obtain the following results:

$$\begin{aligned} \overline{u}(y,s) = {} & \frac{\sinh[y\sqrt{w(s)}]}{s\sinh[\sqrt{w(s)}]} + \frac{s+e_1}{e_0 s[p(s)-w(s)]}\left[\frac{a_3 p(s)(s+d_1)}{s[d_0 p(s)-s-d_1]} - a_2(1+\lambda s)\right]\left[\frac{\sinh[y\sqrt{p(s)}]}{s\sinh[\sqrt{p(s)}]} - \frac{\sinh[y\sqrt{w(s)}]}{s\sinh[\sqrt{w(s)}]}\right] \\ & + \frac{a_3 d_0(s+e_1)}{e_0 s[s+d_1-d_0 w(s)]}\left[1 + \frac{a_7 p(s)(s+d_1)}{s[d_0 p(s)-s-d_1]}\right]\left[\frac{\sinh[y\sqrt{w(s)}]}{s\sinh[\sqrt{w(s)}]} - \frac{\sinh\left[y\sqrt{((s+d_1)/d_0)}\right]}{s\sinh\left[\sqrt{((s+d_1)/d_0)}\right]}\right], \end{aligned} \tag{29}$$

$$\overline{\theta}(y,s) = \frac{\sinh[y\sqrt{p(s)}]}{s\sinh[\sqrt{p(s)}]}, \tag{30}$$

$$\overline{C}(y,s) = \frac{\sinh\left[y\sqrt{((s+d_1)/d_0)}\right]}{s\sinh\left[\sqrt{((s+d_1)/d_0)}\right]} + \frac{a_7 p(s)(s+d_1)}{s[d_0 p(s)-s-d_1]}\left[\frac{\sinh\left[y\sqrt{((s+d_1)/d_0)}\right]}{s\sinh\left[\sqrt{((s+d_1)/d_0)}\right]} - \frac{\sinh[y\sqrt{p(s)}]}{s\sinh[\sqrt{p(s)}]}\right], \tag{31}$$

where

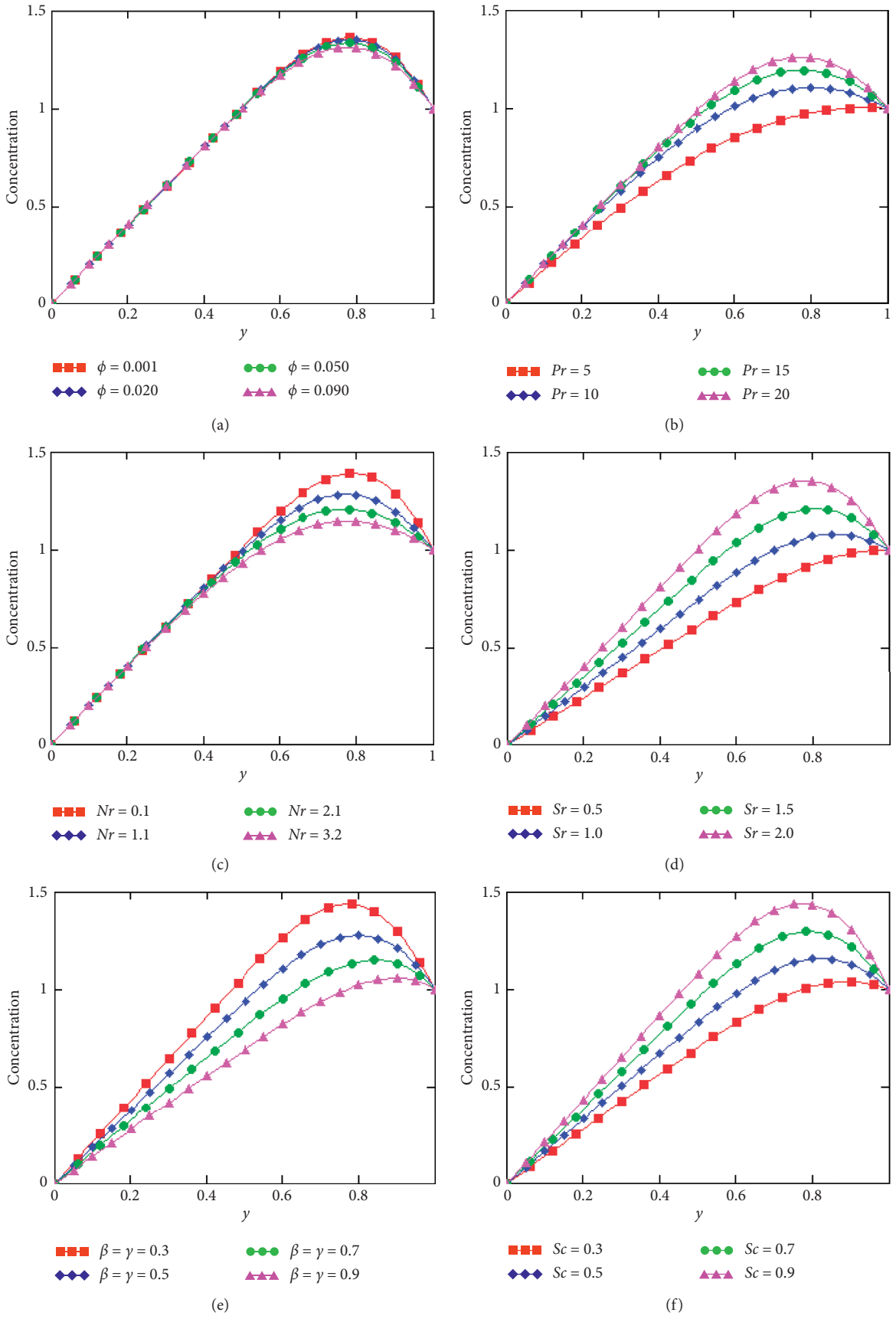

Figure 2: Continued.

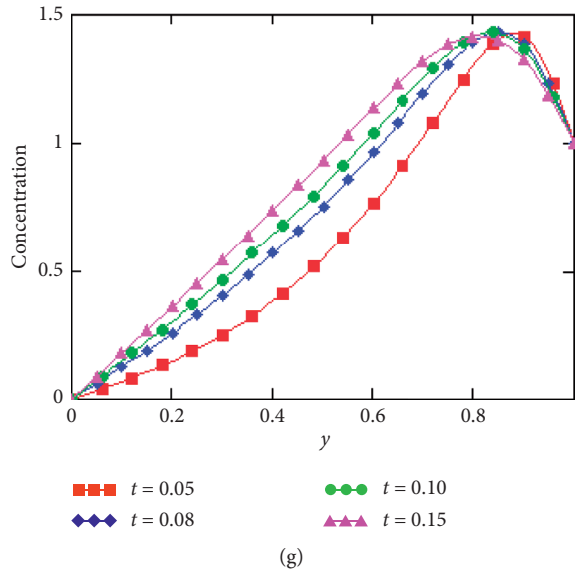

(g)

Figure 2: Variation of concentration.

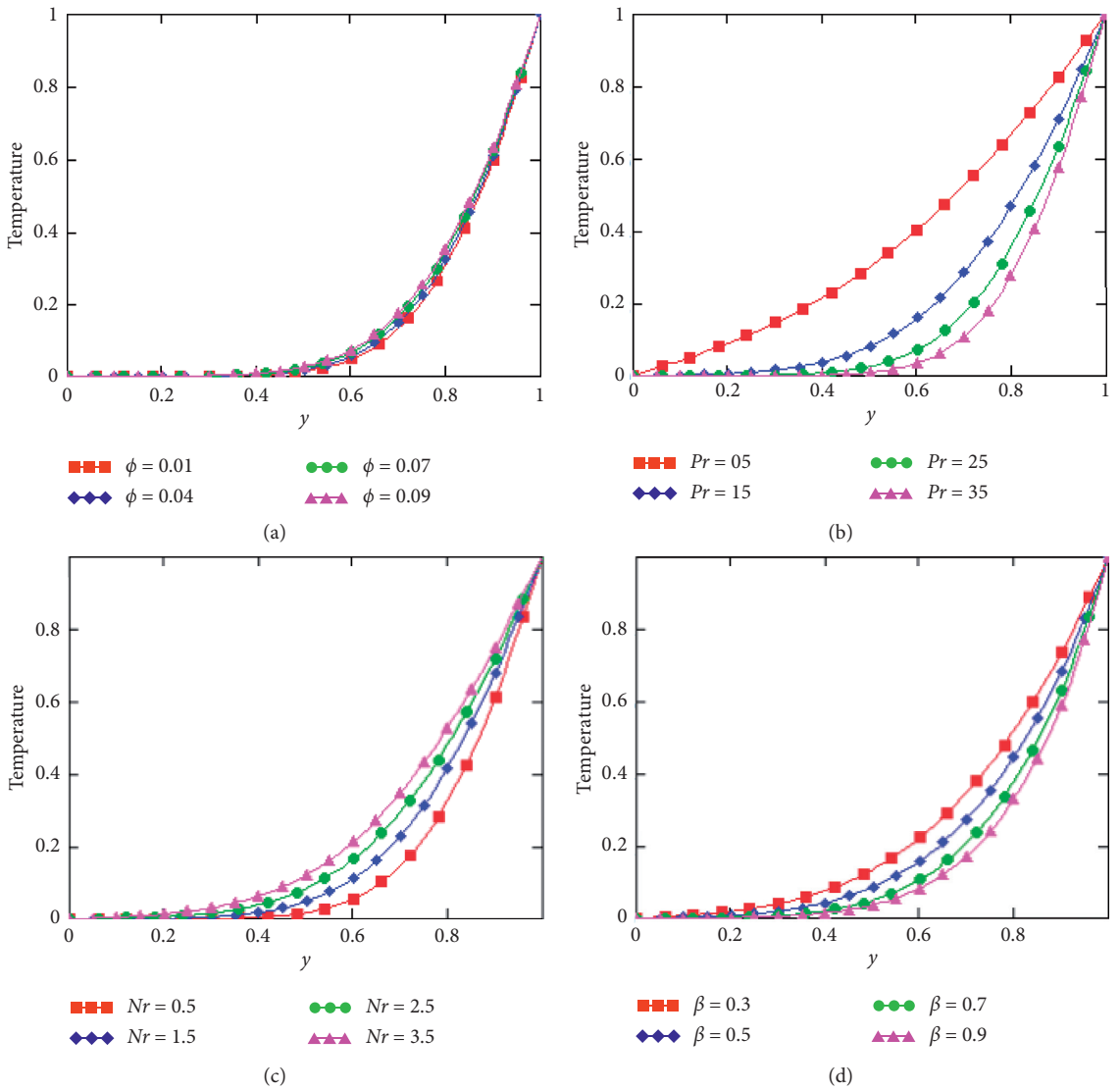

(a) (b) (c) (d)

Figure 3: Continued.

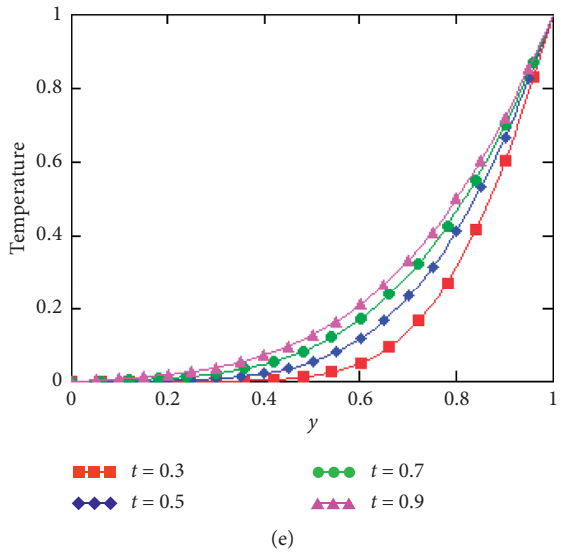

(e)

Figure 3: Variation of temperature.

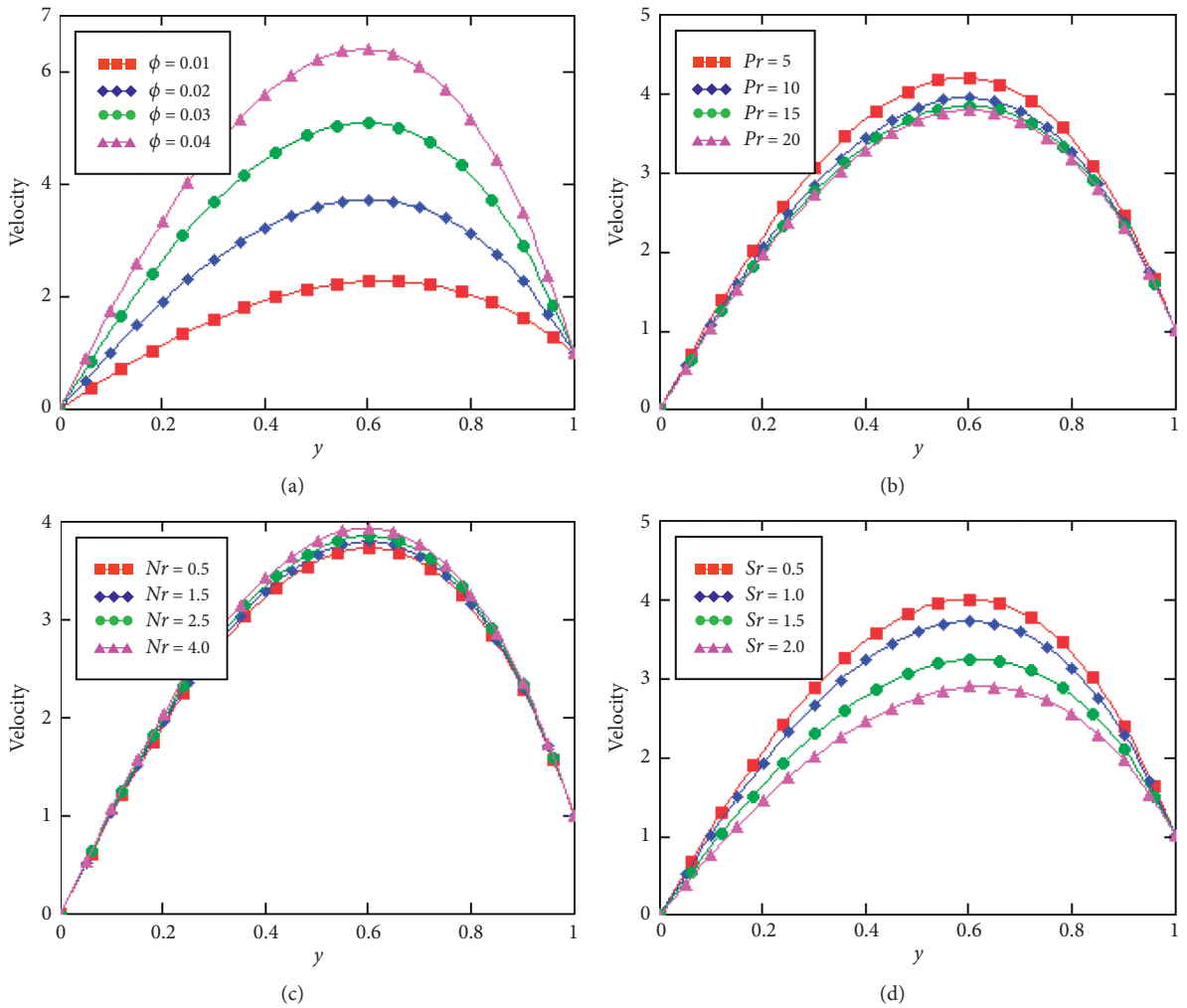

(a) (b) (c) (d)

Figure 4: Continued.

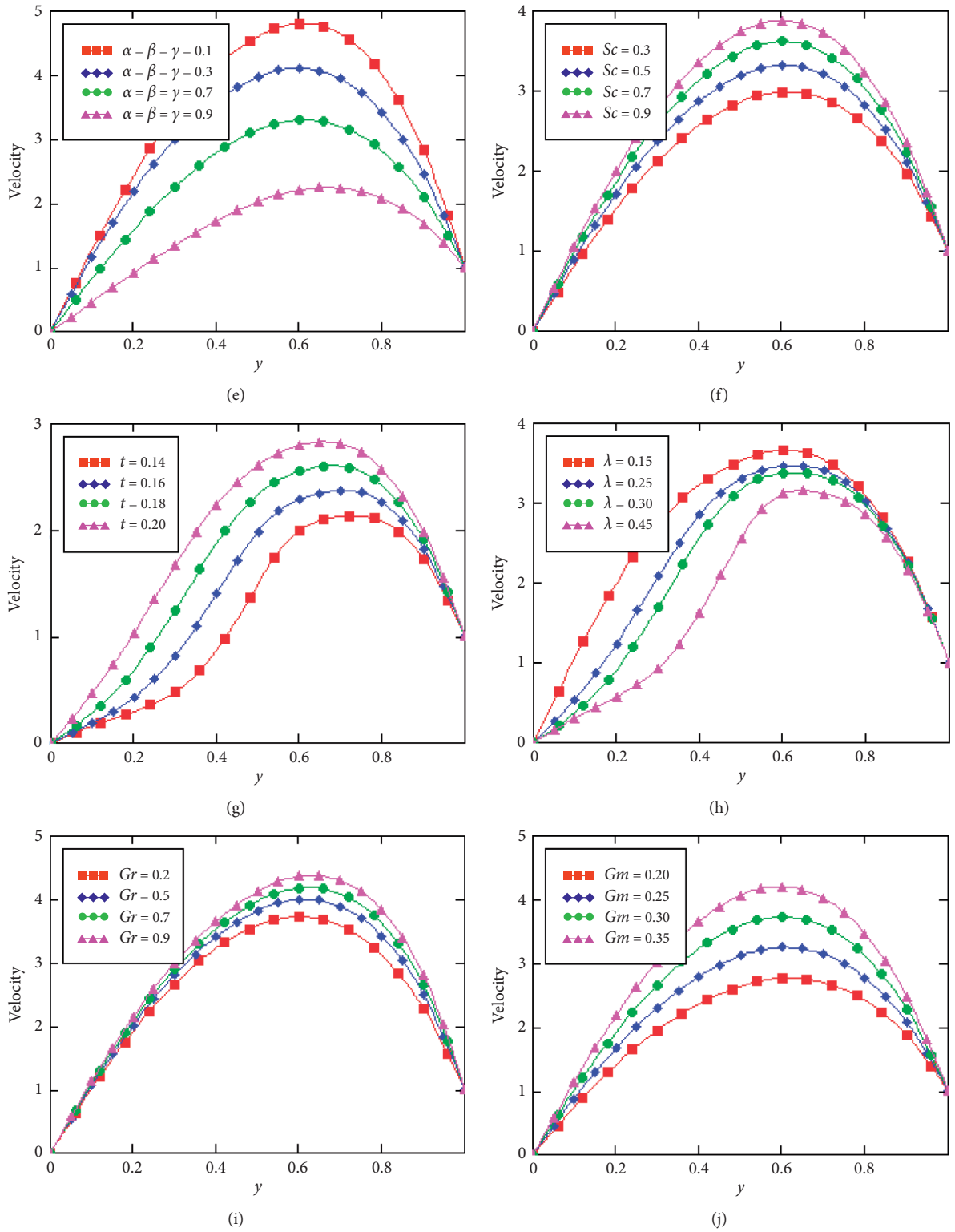

Figure 4: Variation of velocity.

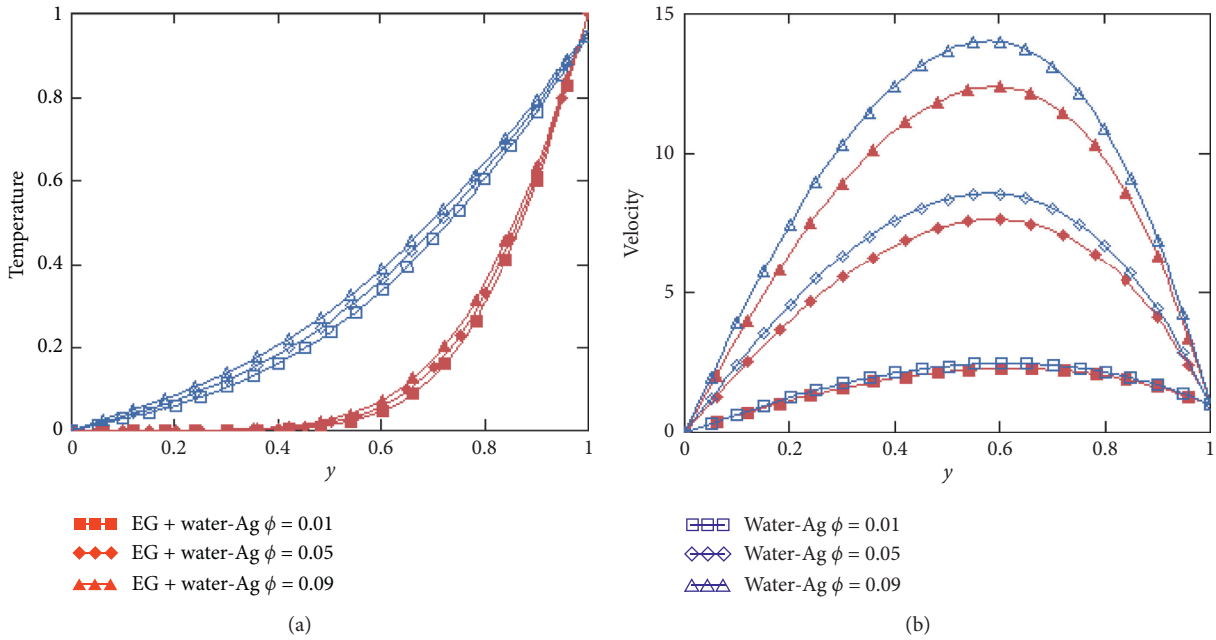

Figure 5: Variation of temperature (a) and velocity (b) of nanofluids.

$$b_0 = \frac{a_4}{1-\beta},$$

$$b_1 = \frac{\beta}{1-\beta},$$

$$p(s) = \frac{s(s+b_1)}{(b_0+a_5)s + a_5 b_1},$$

$$e_0 = \frac{a_1}{1-\alpha},$$

$$e_1 = \frac{\alpha}{1-\alpha},$$

$$w(s) = \frac{(s+e_1)(1+\lambda s)}{e_0},$$

$$d_0 = \frac{a_6}{1-\gamma},$$

$$d_1 = \frac{\gamma}{1-\gamma}. \tag{32}$$

To obtain the inverse of equations (29)–(31) numerically, Stehfest's algorithm [26] is used.

$$u(y,t) \approx \frac{\ln(2)}{t} \sum_{j=1}^{2p} \mathrm{d}_j \overline{u}\left(y, j\frac{\ln(2)}{t}\right), \tag{33}$$

where

$$d_j = (-1)^{j+p} \sum_{i=\lfloor (j+1)/2 \rfloor}^{\min(j,p)} \frac{i^p (2i)!}{(p-i)!\,i!\,(i-1)!\,(j-1)!\,(2i-j)!}, \tag{34}$$

where p is a positive integer.

4. Graphical Results and Discussion

In this section, the graphical analysis of temperature, concentration, and velocity profiles for fractional and flow parameter is carried out in detail. The fractional fluid model is solved by means of the Laplace transform method. Semianalytical results for concentration, temperature, and velocity fields are computed by applying the Laplace inversion numerical algorithm, namely, Stehfest's.

The results obtained shows the influences of the nondimensional governing parameters, namely, Maxwell fluid parameter (λ), nanoparticles volume parameters (ϕ), mass and thermal Grashof numbers (Gm and Gr), Soret effect (Sr), radiation parameter (Nr), Prandtl number (Pr), Schmidt number (Sc), and fractional parameters (α, β, γ) on the flow, temperature, and concentration profiles and are discussed and presented graphically in Figures 2–4. For numerical results, we used $Sc = 0.78$, $\lambda = 0.1$, $\phi = 0.02$, $\alpha = \beta = \gamma = 0.4$, $Sr = 2$, $Pr = 29.86$, $Gr = 0.2$, $Nr = 0.4$, $Gm = 0.3$, and $t = 0.3$. These values are kept common in entire study except the varied values in respective figures. Thermophysical properties of base fluids ($EG + H_2O$) and nanoparticle Ag are given in Table 1.

Figures 2(a), 3(a), and 4(a) depict the effect of volume fraction of nanoparticle ϕ on concentration, temperature, and velocity profiles for ($EG + H_2O$)–Ag nanofluid. It is observed from figures that increase in volume fraction of nanoparticle decreases the concentration profile while increasing the velocity and temperature profiles of the flow. Generally increase in volume fraction of nanoparticles improves the thermal conductivity which makes the fluid hot. These improve the thermal boundary layer thickness along with velocity boundary layers.

Figures 2(b), 3(b), and 4(c) represent the effect of Prandtl number Pr on concentration, temperature, and velocity profiles. It is clear from figures that a raise in the value of Pr enhances the concentration profile and reduces the temperature and velocity profiles. As expected, it is due to the fact that increase in the values of Pr reduces the thermal conductivity making fluid more thick and reducing thickness of thermal boundary layer. Figures 2(c), 3(c), and 4(c) illustrate the effect of radiation parameter Nr on concentration, velocity, temperature, and velocity profiles. We observed from figures that increase in Nr decreases the concentration profile while increasing the velocity and temperature profiles of the flow. Clearly, with the increase in the values of Nr, the amount of heat transfers to the fluid increases which increases the temperature of the fluid and in turn enhances the flow of fractional nanofluid. Figures 2(d) and 4(d) depict the effect of Soret Sr on concentration and velocity profiles. It can be seen from figures that increase in Sr decreases the concentration profile while increasing the velocity profiles of the flow.

Figures 2(e), 3(d), and 4(e) symbolize the effect of fractional parameters α, β, and γ on concentration, temperature, and velocity profiles. It is obvious from figures that raise in the values of α reduces the concentration, temperature, and velocity profiles. Figures 2(f) and 4(f) represent the effect of Schmidt number Sc on concentration and velocity profiles. It is evident from figures that a raise in the value of Sc enhances the concentration and velocity profiles. Figures 2(g), 3(e), and 4(g) represent the effect of time t on concentration, temperature, and velocity profiles. From these figures, it is observed that concentration, temperature, and velocity increases for increasing values of t.

Figure 4(h) signifies the effect of Maxwell fluid parameter λ on velocity profile. This figure shows that the velocity is a decreasing function λ.

Figures 5(a) and 5(b) show a comparison of two different nanofluids when nanoparticles of Ag were added to the two kings of base fluids EG + H_2O and H_2O. It is interesting to mention that the enhancement in temperature and velocity profiles of H_2O–Ag nanofluid is more than that of EG + H_2O–Ag nanofluid.

5. Conclusions

In this study, we analyzed the influence of thermal radiation and Soret parameters of an unsteady Maxwell fractional nanofluid flow in a vertical channel by considering EG + water (50 : 50)-Ag and water-Ag nanofluids. The fractionalized governing equations modeled with Caputo–Fabrizio time fractional derivative are solved via the Laplace transform method. Numerical inversion Laplace transforms technique, namely, Stehfest's is used in MATHCADE software to find the inverse Laplace transform for concentration, temperature, and velocity graphically. Some important outcomes of this study are as follows:

(1) The EG + water based Maxwell nanofluid has lesser heat transfer rate than water-based nanofluid

(2) The heat transfer rate enhances with the higher concentration of nanoparticles

(3) The velocity reduces for higher values of Maxwell fluid parameterλ

(4) Temperature and velocity of the fluid can be controlled by using volume fraction and also by using mixture of conventional fluids as base fluid

(5) Greater values of volume fraction ϕ demonstrated considerable effect on mass, energy, and momentum profiles

(6) The influence of Gr and Gm stabilizes the growth of momentum boundary layer

(7) The existence of Sr and substantial species increases the concentration

(8) The suspension of nanoparticles in EG + water provides a potential in increasing the heat transport performance

Nomenclature

$\widetilde{u}$: Velocity (m/s)
$\widetilde{C}$: Concentration (kg/m^3)
$\widetilde{T}$: Temperature (K)
g: Gravitational acceleration (m/s^2)
k: Thermal conductivity (W/m K)
D: Mass diffusivity (m^2/s)
c_p: Specific heat (J/kg K)
Gr: Thermal Grashof number
Nr: Thermal radiation
Gm: Mass Grashof number
Sc: Schmidt number
Sr: Soret effect
Pr: Prandtl number.

Greek Symbols

$\widetilde{\lambda}$: Maxwell fluid parameter
λ: Dimensionless parameter
μ: Dynamic viscosity (kg/m s)
σ: Electric conductivity (S/m)
ρ: Density (kg/m^3)
ν: Kinematic viscosity (m^2/s)
$k\prime$: Absorption coefficient
k_T: Thermal diffusion
$\sigma\prime$: Stefan Boltzmann constant
T_m: Mean temperature
β_T: Thermal expansion coefficient (K^{-1})
θ: Dimensionless temperature
β_C: Mass volumetric coefficient (K^{-1})
ϕ: Volume fraction.

Subscript

nf: Nanofluid
f: Fluid.

Data Availability

The data used to support the findings of this study are available from the corresponding author upon request.

Conflicts of Interest

The authors declare that there are no conflicts of interest regarding the publication of this paper.

References

[1] W. N. Mutuku and O. D. Makinde, "On hydromagnetic boundary layer flow of nanofluids over a permeable moving surface with Newtonian heating," *Latin American Applied Research*, vol. 44, no. 1, pp. 57–62, 2014.

[2] A. J. Omowaye, A. I. Fagbade, and A. O. Ajayi, "Dufour and Soret effects on steady MHD convective flow of a fluid in a porous medium with temperature dependent viscosity: homotopy analysis approach," *Journal of the Nigerian Mathematical Society*, vol. 34, no. 3, pp. 343–360, 2015.

[3] S. S. K. Raju, M. Narahari, and P. Rajashekhar, "Soret and chemical reaction effects on unsteady two-dimensional natural convection along a vertical plate," *AIP Conference Proceedings*, vol. 1621, p. 154, 2014.

[4] G. V. R. Reddy, "Soret and Dufour Effects on MHD free convective flow past a vertical porous plate in the presence of heat generation," *International Journal of Applied Mechanics and Engineering*, vol. 21, no. 3, pp. 649–665, 2016.

[5] D. R. Srinivas, G. S. Sreedhar, and K. Govardhan, "Effect of viscous dissipation, Soret and Dufour effect on free convection heat and mass transfer from vertical surface in a porous medium," *Procedia Materials Science*, vol. 10, pp. 563–571, 2015.

[6] S. Tippa, M. Narahari, and P. Rajashekhar, "Dufour effect on unsteady natural convection flow past an infinite vertical plate with constant heat and mass fluxes," *AIP Conference Proceedings*, vol. 1621, p. 470, 2014.

[7] I. J. Uwanta and H. Usman, "On the influence of Soret and Dufour effects on MHD free convective heat and mass transfer flow over a vertical channel with constant suction and viscous dissipation," *International Scholarly Research Notices*, vol. 2014, Article ID 639159, 11 pages, 2014.

[8] C. RamReddy, P. V. S. N. Murthy, A. J. Chamkha, and A. M. Rashad, "Soret effect on mixed convection flow in a nanofluid under convective boundary condition," *International Journal of Heat and Mass Transfer*, vol. 64, pp. 384–392, 2013.

[9] C. S. K. Raju, M. J. Babu, N. Sandeep, V. Sugunamma, and J. V. R. Reddy, "Radiation and Soret effects of MHD nanofluid flow over a moving vertical moving plate in porous medium," *Chemical and Process Engineering Research*, vol. 30, pp. 9–23, 2015.

[10] N. V. Ganesh, Q. M. Al-Mdallal, K. Reena, and S. Aman, "Blasius and Sakiadis slip flow of H2O-C2H6O2 (50:50) based nanoliquid with different geometry of boehmite alumina nanoparticles," *Case Studies in Thermal Engineering*, vol. 16, Article ID 100546, 2019.

[11] A. A. A. Arani, S. Sadripour, and S. Kermani, "Nanoparticle shape effects on thermal-hydraulic performance of boehmite alumina nanofluids in a sinusoidal-wavy mini-channel with phase shift and variable wavelength," *International Journal of Mechanical Sciences*, vol. 128-129, pp. 550–563, 2017.

[12] M. Monfared, A. Shahsavar, and M. R. Bahrebar, "Second law analysis of turbulent convection flow of boehmite alumina nanofluid inside a double-pipe heat exchanger considering various shapes for nanoparticle," *Journal of Thermal Analysis and Calorimetry*, vol. 135, no. 2, pp. 1521–1532, 2019.

[13] K. S. Nisar, U. Khan, A. Zaib, I. Khan, and D. Baleanu, "Numerical simulation of mixed convection squeezing flow of a hybrid nanofluid containing magnetized ferroparticles in (50%:50%) of ethylene glycol–water mixture base fluids between two disks with the presence of a non-linear thermal radiation heat flux," *Frontiers Chemistry*, vol. 8, p. 792, 2020.

[14] M. Saqib, I. Khan, and S. Shafie, "Application of Atangana-Baleanu fractional derivative to MHD channel flow of CMC-based-CNT's nanofluid through a porous medium," *Chaos, Solitons & Fractals*, vol. 116, pp. 79–85, 2018.

[15] N. Makris, G. F. Dargush, and M. C. Constantinou, "Dynamic analysis of generalized viscoelastic fluids," *Journal of Engineering Mechanics*, vol. 119, no. 8, pp. 1663–1679, 1993.

[16] A. A. Zafar and C. Fetecau, "Flow over an infinite plate of a viscous fluid with non-integer order derivative without singular kernel," *Alexandria Engineering Journal*, vol. 55, no. 3, pp. 2789–2796, 2016.

[17] I. Siddique and S. M. Bukhari, "Analysis of the effect of generalized fractional Fourier's and Fick's laws on convective flows of non-Newtonian fluid subject to Newtonian heating," *The European Physical Journal Plus*, vol. 135, no. 1, pp. 1–21, 2020.

[18] B. S. T. Alkahtani and A. Atangana, "Modeling the potential energy field caused by mass density distribution with eton approach," *Open Physics*, vol. 14, no. 1, pp. 106–113, 2016.

[19] I. Siddique, I. Tlili, S. M. Bukhari, and Y. Mahsud, "Heat transfer analysis in convective flows of fractional second grade fluids with Caputo–Fabrizio and Atangana–Baleanu derivative subject to Newtonion heating," *Mechanics of Time-dependent Materials*, pp. 1–21, 2020.

[20] K. A. Abro, I. Khan, and J. F. Gómez-Aguilar, "A mathematical analysis of a circular pipe in rate type fluid via Hankel transform," *The European Physical Journal Plus*, vol. 133, no. 10, p. 397, 2018.

[21] I. Siddique, N. A. Shah, and K. A. Abro, "Thermography of ferromagnetic Walter's-B fluid through varying thermal stratification," *South African Journal of Chemical Engineering*, vol. 36, pp. 118–126, 2021.

[22] D. Vieru, C. Fetecau, and C. Fetecau, "Time-fractional free convection flow near a vertical plate with Newtonian heating and mass diffusion," *Thermal Science*, vol. 19, no. 1, pp. 85–98, 2015.

[23] M. Ahmad, M. A. Imran, and M. Nazar, "Mathematical modeling of (Cu-Al2O3) water based Maxwell hybrid nanofluids with Caputo-Fabrizio fractional derivative," *Advances in Mechanical Engineering*, vol. 12, no. 9, pp. 1–11, 2020.

[24] S. Kakac and A. Pramuanjaroenkij, "Review of convective heat transfer enhancement with nanofluids," *International Journal of Heat Mass Transfer*, vol. 52, no. 13-14, pp. 3187–3196, 2009.

[25] M. Caputo and M. Fabrizio, "A new definition of fractional derivative without singular kernel," *Progress in Fractional Differentiation and Applications*, vol. 1, no. 2, pp. 73–85, 2015.

[26] H. Stehfest, "Algorithm 368: numerical inversion of Laplace transforms [D5]," *Communications of the ACM*, vol. 13, no. 1, pp. 47–49, 1970.